Eur. Phys. J. D (2015) 69: 205
DOI: 10.1140/epjd/e2015-60063-2

THE EUROPEAN PHYSICAL JOURNAL D

Regular Article

Simulation of the plasma sheath dynamics in a spherical plasma focus

Yasar Ay[1,a], Mohamed A. Abd Al-Halim[2], and Mohamed A. Bourham[1]

[1] Department of Nuclear Engineering, North Carolina State University, Raleigh, NC 27695-7910, USA
[2] Department of Physics, Benha University, 13518 Benha, Egypt

Received 31 January 2015 / Received in final form 15 May 2015
Published online 3 September 2015 –

Abstract. A two concentric electrodes spherical plasma focus device is simulated using a snow plow model, depending on the momentum, circuit and shock wave equations. In the spherical plasma focus, the magnetic pressure for constant discharge current is higher at the system antipodal point as compared to that at the equator. The simulation phases include a run down phase with expansion from the first antipodal to the equator, then a compression from the equator point to the second antipodal point, and finally a reflection of the shock wave on the axis. The results show that the spherical plasma focus model is in good agreement with published experimental results of the plasma parameters such as the discharge current and current derivative. Plasma parameters and the effect of the variation in the gas pressure and discharge voltage were obtained for hydrogen, deuterium and tritium. The energy deposited into the plasma sheath and the power deposited into the plasma focus tube are calculated. The basic calculation of the current fraction is also included in this study.

1 Introduction

Plasma Focus (PF) devices are pulsed devices that were independently developed by Filippov [1] and Mather [2,3] in a cylindrical geometry with the different electrode configurations. The PF devices are used to produce hot and dense plasma sources through an electric discharge occurring across the surface of the insulator, followed by the formation of an axially symmetric current sheath (CS). Plasma focus devices are useful for various purposes, such as x-ray production [4,5], neutron production [4,6–11] and nuclear fusion reactions [12–14].

Several models were developed for both Mather type [15–23] and Flippov type [24–26] plasma focus devices. The most used and known model for the Mather type PF is Lee's snowplow in the axial phase and the Potter's slug model [27,28] in the radial phases due to the zero final radius of the snow plow model in the radial phases and coupled them with the plasma circuit equations. In addition to the plasma focus dynamics, Lee's model successfully simulates various important parameters such as the energy transfer process in the PF [29], and dimension and lifetime of the pinch [15,30]. In Lee's model, the electric current that pass through the plasma sheath is considered a fraction of the total discharge current, which is represented as the current fraction factor in Lee's model. Even if it is the case in this study, it is not necessary for a lumped parameter model [31]. It is also not a requirement for advanced models [32–35].

A model was also developed by Abd Al-Halim for PF with hemispherical electrodes [36]. In this model, the snowplow approximation together with the momentum equation, the plasma circuit equation and the shock wave equations were used.

In this hemispherical model, the motion starts at the equator and ends at the antipodal point of the hemisphere. The governing equations of this model is equation of motion, which consists of the momentum and magnetic pressure equation to calculate the plasma sheath velocity and position. It also includes the circuit equation, which is used to calculate the plasma inductance and discharge voltage. In order to calculate the plasma temperature and shock wave velocity with its position, the shock wave equation is used. In this study, the comparison between hemispherical electrodes and cylindrical electrodes were investigated. A good match of discharge current between hemispherical and cylindrical electrodes were obtained for validation. The deep dip current and sharp spike voltage represent the evidence of better focusing formations [37–39]. Hemispherical electrodes has a dipper discharge current dip with the higher discharge voltage spike, which shows better focus action for hemispherical electrodes plasma focus device compared to cylindrical electrodes one. Better focus represents optimum conditions which is the radiation emission in the case of plasma focus devices, such as X-ray production [40,41] or neutron production [42,43]. The hemispherical model was not compared to any experimental work since no experimental data was available at that time.

[a] e-mail: yay@ncsu.edu

For the Mather type PF, the Masoud model [20] has introduced an angle into the snow plow model, slug model and plasma circuit equations in order to improve the continuity between the axial and radial phases for the calculation of the plasma parameters.

The open-cathode PF model, which is the PF without surrounding cathode, was developed to predict the neutron production and pinch voltage of the PF [21,22]. This model was based on the snowplow model in addition to the included pinch model. The three-phase theory model has allowed the CS to have both radial and axial variation during the rundown phase [23]. This model also accounts the breakdown of the gas. A three-stage model was used to predict the design parameters, such as inner and outer electrode radii, and inner electrode length in addition to the gas pressure and charging voltage for optimum focus.

For the Filippov type PF, while Siahpoush et al. [25] has adapted the Lee model with the slug model for Filippov type PF, Goudarzi et al. has used the lumped parameter model with the mass and momentum equations coupled with the equivalent circuit equations [26].

The main objective of this work is to develop a plasma focus model which consists of rundown phase I, rundown phase II and reflected shock phase for a spherical plasma focus device, and validate the developed model versus experimental results. The snow plow model with the help of the shock wave equations coupled to the circuit equations is used to predict the plasma and shock wave parameters in the spherical plasma focus device. The set of equations describing the developed model are solved with the linear approximation method [36].

The model is able to predict the temporal evolution of the current, inter-electrode voltage, and temperature and velocity of the current sheet.

The model was also run to gain insight on the effect of the gas pressure and discharge voltage on plasma temperature and pinch start time for hydrogen, deuterium and tritium.

2 Spherical plasma focus model

A model for the spherical plasma focus (SPF) device has been developed, which consists of three phases: a rundown phase I, a rundown phase II and a reflected shock phase. Figure 1 illustrates the configuration of the SPF showing the inner and outer electrodes, the insulator, the CS and the equivalent circuit model which consists of the circuit inductance L_0, resistance r_0, the capacitor bank C_0, and the closing switch.

While the angle of the motion varies first from one antipodal point to the equator point then to the other antipodal point resulting in 3 phases which are a rundown phase I with sheath expansion, a rundown phase II with sheath compression and the reflected shock phase in the spherical case, the hemispherical case has one phase due to the different electrode shape which has angle varying from equator point to the antipodal point. Since the shape is spherical, the angle of the plasma sheath and the angle variation are important factors for the motion of the

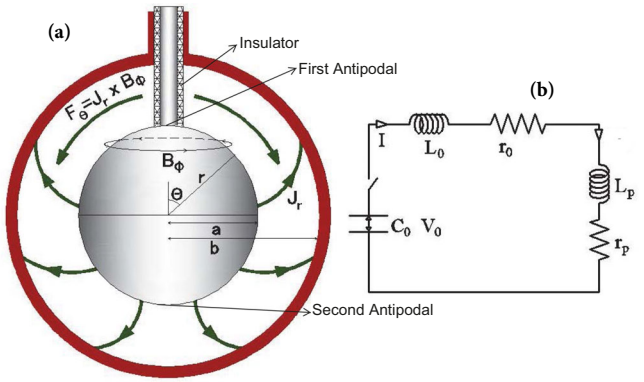

Fig. 1. (a) Spherical plasma focus configuration. (b) Equivalent circuit model of the SPF.

plasma sheath and related parameters which can be seen, for example, in equations (10) and (29) for the plasma sheath motion, equations (8) and (28) for the magnetic field, equations (14) and (30) for the plasma inductance. A clear plateau is observed in the results of the velocity and temperature while the current increases. Such behavior was not observed in the results of the hemisphere model.

In order to produce a pinched high density-high temperature plasma, the first step is to form the current sheath (CS) across the insulator surface and to accelerate the CS down the discharge tube followed by radial compression to produce the pinch. Filippov and Mather type PF's used PF geometries as design concepts with some differences. For example, while the radial compression phase starts after the axial (run-down) phase in Mather's type, it starts with the formation of the CS in Filippov's type PF. The spherical plasma focus (SPF) has different features compared with Mather and Filippov type PF devices due to geometrical configuration. In the spherical plasma focus devices while the CS is accelerated with the CS expansion in the rundown phase (phase I), it is compressed in both radial and axial directions in the rundown phase (phase II) and the reflected shock phase.

The symmetric umbrella-like shape of the CS is produced by the gas discharge between the electrodes across the insulator surface. The increasing current density J, which is flowing through the electrodes and the CS, creates an azimuthal magnetic field B which results in the CS lifts off from the insulator. Radially flowing current J_r and induced azimuthal magnetic field B_ϕ produces a $J \times B$ force. The $J \times B$ force accelerates the CS in the direction shown in Figure 1 with an angle θ towards the first equator point and then the other antipodal point [36]. Since magnetic field is changing during the CS motion and the CS is supersonic, an ionizing shock wave (shock front) ionizes the undisturbed gas ahead of the shock wave. This produced shock front collects the ionized gas particles like a solid magnetic piston with some mass efficiency factor f_m.

A plasma layer is assumed to exist between the current sheath and the shock front, which is called the slug, and the gas inside the slug is assumed to be homogeneous and ionized. Plasma slug temperature is calculated with the help of the shock front velocity by considering uniform

pressure between the magnetic piston and the shock front. After the CS reaches the equator point which has the lowest magnetic field and the lowest magnetic pressure, the magnetic field and magnetic pressure start to increase which results in accelerating the CS towards the axis. Since the shock front is formed in front of the CS and has higher speed, the shock front reaches the axis and reflects back towards the CS. When the reflected shock front hits the CS, the CS continues to move towards the axis. Thereafter, the current sheath collapses on the axis and forms the pinch (small dense plasma) which has a high temperature and high energy density.

2.1 Rundown phase I

The rundown phase I will start immediately after the gas breakdown. The snowplow model with the shock wave equations is used to calculate the plasma and shock parameters in this phase. It is assumed that the CS moves perpendicular to the direction of acceleration. The equations used for plasma sheath motion in the rundown phase I are the momentum, magnetic force and the circuit equations.

2.1.1 Insulator volume calculation

Since the insulator has considerable effect on plasma parameters, its volume should be taken into account.

$$V_{ins} = \int_0^{2\pi} d\phi \int_a^b r^2 dr \int_0^{\theta_0} \sin\theta_0 d\theta = \frac{2\pi}{3}\left(b^3 - a^3\right)\left(1 - \cos\theta_0\right) \quad (1)$$

where V_{ins} is the insulator volume corresponding to the angle θ_0, ϕ is the azimuthal angle, r is the radial distance at which the plasma parameters are calculated. θ is the polar angle, which is a function of the discharge time t, b and a are the outer and inner electrode radii, respectively.

2.1.2 Effective volume calculation

Since the CS sweeps all the gas in front of it, the volume at which point the plasma sheath reaches should be considered for mass calculation in order to get correct plasma sheath parameters. Therefore, volume at which plasma sheath parameters are calculated is:

$$V_{\text{eff}} = \int_0^{2\pi} d\phi \int_a^b r^2 dr \int_0^{\theta} \sin\theta d\theta - V_{ins}, \quad (2)$$

$$V_{\text{eff}} = \frac{2\pi}{3}\left(b^3 - a^3\right)\left(1 - \cos\theta\right) - V_{ins}. \quad (3)$$

Then

$$V_{\text{eff}} = \frac{2\pi}{3}\left(b^3 - a^3\right)\left(\cos\theta_0 - \cos\theta\right). \quad (4)$$

The present study assumes that there is no effect for the insulator since its dimension is too small as compared to the whole sphere, hence the motion is considered to start at angle theta which is very small and close to zero.

2.1.3 Momentum equation

Since the flowing current J and induced magnetic field B produces the $J \times B$ force which acts on the current sheath as magnetic force P_B, then the rate of momentum change of the CS can be determined by the magnetic force. The force due to the rate of momentum change of the CS in the rundown phase I is:

$$F_1 = \frac{d(mv_\theta)}{dt}, \quad (5)$$

where $v_\theta = r\dot{\theta}$ is the tangential velocity, and $m = \rho f_m \frac{2\pi}{3} \times (b^3 - a^3)(\cos\theta_0 - \cos\theta)$ is the mass of the plasma sheath, and hence

$$F_1 = \rho f_m \frac{2\pi}{3}(b^3 - a^3) r[\sin\theta\dot{\theta}^2 + (\cos\theta_0 - \cos\theta)\ddot{\theta}], \quad (6)$$

where ρ is the initial gas density and f_m is the fraction of mass swept up by the sheath motion. The magnetic force F_2 on the current sheath can be determined from the magnetic pressure P_B

$$F_2 = \int_a^b P_B dA = \int_a^b \frac{B^2}{2\mu_0} dA, \quad (7)$$

where

$$B = \frac{\mu_0 I f_c}{2\pi r \sin\theta}, \quad (8)$$

is the magnetic field at distance r due to the current I flowing in the CS with the f_c current fraction that accounts for the current shedding effect, μ_0 is permeability of free space and $dA = 2\pi r \sin\theta dr$ is the small area of the sheath over which the magnetic field is calculated, then,

$$F_2 = \frac{\mu_0 I^2 f_c^2}{4\pi \sin\theta} \ln\left(\frac{b}{a}\right). \quad (9)$$

Since the rate of momentum change of the CS is equal to the magnetic force on the current sheath, F_1 is set equal to F_2, and it is solved for $\ddot{\theta}$ to find the equation of motion in the rundown phase I:

$$\ddot{\theta} = \frac{\alpha^2 I^2}{r \sin\theta(\cos\theta_0 - \cos\theta)} - \frac{\dot{\theta}^2 \sin\theta}{\cos\theta_0 - \cos\theta}, \quad (10)$$

where α is the scaling parameter which is given by

$$\alpha^2 = \frac{3\mu_0 f_c^2 \ln(b/a)}{8\pi^2 \rho f_m (b^3 - a^3)}. \quad (11)$$

The sheath velocity is obtained by integrating the acceleration equation (Eq. (10)) then the sheath position is obtained by integration of the velocity.

2.1.4 Plasma inductance

The magnetic flux and the plasma inductance can be calculated as follows:

$$\phi_B = \int_a^b B dA = \int_a^b \frac{\mu_0 I f_c}{2\pi r \sin\theta} r(\theta - \theta_0) dr, \quad (12)$$

where ϕ_B is the magnetic flux, and $dA = \ell dr = r(\theta - \theta_0)dr$ is the area over which the inductance is calculated, ℓ is the arch length at which point the inductance is calculated. The plasma inductance is given by

$$L = \frac{\phi_B}{If_c} = \int_a^b \frac{\mu_0}{2\pi r \sin\theta} r(\theta - \theta_0)dr = \frac{\mu_0(b-a)}{2\pi}\frac{(\theta - \theta_0)}{\sin\theta}. \tag{13}$$

The plasma inductance can be written in terms of the scaling parameter β as follows:

$$L = \frac{\beta(\theta - \theta_0)}{f_c \sin\theta}, \tag{14}$$

where

$$\beta = \frac{\mu_0(b-a)f_c}{2\pi} \tag{15}$$

and the inductance derivative is

$$\frac{dL}{dt} = \frac{\beta\dot{\theta}}{f_c \sin\theta}[1 - (\theta - \theta_0)\cot\theta]. \tag{16}$$

2.1.5 Discharge current

General assumption is to ignore the plasma resistance $r(t)$ when calculating the circuit equation. The current can be calculated by using Kirchhoff's Law according to Figure 1b:

$$\frac{d}{dt}[(L_0 + Lf_c)I] + r_0 I = V_0 - \int \frac{Idt}{C_0}, \tag{17}$$

$$(L_0 + Lf_c)\frac{dI}{dt} + If_c\frac{dL}{dt} + r_0 I = V_0 - \int \frac{Idt}{C_0}, \tag{18}$$

$$\frac{dI}{dt} = \frac{V_0 - \int \frac{Idt}{C_0} - r_0 I - If_c\frac{dL}{dt}}{L_0 + Lf_c}. \tag{19}$$

2.1.6 Discharge voltage

The discharge voltage for spherical plasma focus (SPF) device can be obtained from the inductive equation:

$$V = \frac{d}{dt}[LIf_c] = f_c I\frac{dL}{dt} + f_c L\frac{dI}{dt}. \tag{20}$$

2.1.7 Shock velocity

While the CS and shock front (constituting plasma slug together) moves from the first antipodal point to the other antipodal point, the plasma slug collects all the gas encountered by the shock front which is assumed to be thin. Therefore, the planar shock-jump equations can be used across the shock front to calculate the shock velocity, which is used to calculate the plasma temperature. Assuming that the shock pressure P_s is uniform across the slug, the shock pressure can be set equal to the magnetic pressure P_B at the magnetic piston to calculate the shock velocity v_s. Shock pressure P_s can be written as follows:

$$P_s = \frac{2}{\gamma + 1}\rho f_m v_s^2, \tag{21}$$

where γ is the specific heat ratio, v_s is the shock velocity. Then the magnetic pressure for the rundown phase is given by

$$P_B = \frac{\mu_0 I^2 f_c^2}{8\pi^2 r^2 \sin^2\theta}. \tag{22}$$

Therefore, the shock velocity is given by:

$$v_s = \frac{dr_s}{dt} = -\frac{If_c}{4\pi r \sin\theta}\sqrt{\frac{\mu_0(\gamma+1)}{\rho f_m}}, \tag{23}$$

where the minus sign represents the motion in the opposite direction.

2.1.8 Plasma energy and power consideration

In the plasma focus system, all the energy comes from the capacitor energy bank E_{tot} which is distributed into the system. The total energy and power can be calculated as follows:

$$E_{\text{tot}} = \frac{1}{2}C_0 V_0^2, \tag{24}$$

$$P_{\text{tot}} = I_0 V_0, \tag{25}$$

where $I_0 = V_0\sqrt{C_0/L_0}$.

The deposited energy into the plasma sheath E_p and the power deposited into tube P_{tube} are calculated as follows:

$$E_p = \int If_c V dt, \tag{26}$$

$$P_{\text{tube}} = IV. \tag{27}$$

2.2 Rundown phase II

The rundown phase II starts when the current sheath reaches the equator point, and it ends when the shock front hits the axis. As in the rundown phase I, the snowplow model with the shock wave equations are used together with necessary modifications for rundown phase II. The same assumptions and set of governing equations are used in this phase to calculate the plasma and shock parameters. Effective volume, discharge current and discharge voltage calculations are the same as in the rundown phase I.

2.2.1 Momentum equation

In the rundown phase II, the magnetic field, which is used for the rundown phase II and the reflected shock phase, is calculated as follows:

$$B = \frac{\mu_0 If_c}{2\pi r\cos(\theta - \pi/2)}. \tag{28}$$

Since the rate of momentum change of the CS is equal to the magnetic force on the current sheath, F_1 is set equal to F_2 in the rundown phase II, and it is solved for $\ddot{\theta}$.

$$\ddot{\theta} = \frac{\alpha^2 I^2}{r\cos(\theta - \pi/2)(\cos\theta_0 - \cos\theta)} - \frac{\sin\theta\dot{\theta}^2}{\cos\theta_0 - \cos\theta}, \quad (29)$$

where the scaling parameter α in the rundown phase II is the same as the scaling parameter in the rundown phase I.

2.2.2 Plasma inductance

Since the magnetic field equation in this phase is calculated as in equation (28), plasma inductance and the derivative of the plasma inductance are calculated as follows:

$$L = \frac{\beta(\theta - \theta_0)}{f_c\cos(\theta - \pi/2)} \quad (30)$$

$$\frac{dL}{dt} = \frac{\beta\dot{\theta}}{f_c\cos(\theta - \pi/2)}[1 + (\theta - \theta_0)\tan(\theta - \pi/2)]. \quad (31)$$

2.2.3 Shock velocity

The shock velocity v_s for the rundown phase II is then written as:

$$v_s = \frac{dr_s}{dt} = -\frac{I f_c}{4\pi r\cos(\theta - \pi/2)}\sqrt{\frac{\mu_0(\gamma + 1)}{\rho f_m}}. \quad (32)$$

2.3 Reflected shock phase

The reflected shock phase starts after the shock front hits the axis, and reflects back towards the CS. It ends when the shock front hits the CS. In this phase the distance between the CS and the shock front starts decreasing as opposed to the rundown phases I and II until the shock front meets the CS. The constant shock front velocity is used in this phase, which is 0.3 times the shock front velocity on the axis when the shock front hits the axis [44]. The same snowplow model and the shock wave equations with the constant shock front velocity are used in this phase. Therefore, the governing equations are the same as in the rundown phase II with the constant reflected shock front velocity, which is given by:

$$v_s = 0.3(v_s)_{on-axis}, \quad (33)$$

where $(v_s)_{on-axis}$ represents the velocity of the shock front when the shock front hits the axis at the end of the rundown phase II [25].

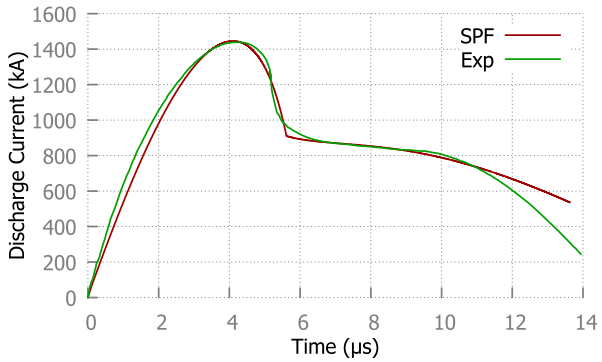

Fig. 2. Calculated and measured total discharge current for DT mixture.

3 Results and discussion

3.1 Model validation

To validate the SPF model, it will be compared with the results of the experiment of a spherical plasma focus chamber [45]. In this study, the plasma focus consists of 2 concentric electrodes, with inner and outer electrode radii of 8 and 14.5 cm, respectively. The capacitor bank, charging voltage, external inductance and the equal amount of DT mixture filling gas pressure are 432 μF, 25 kV, 36 nH, and 14.5 Torr, respectively. The resistance is used to control the value of the current peak, but it usually has small values and has lower effect as compared to the other parameters like the inductance and could be neglected in some cases. In this study, the best value of the resistance r_0 is 3.2 mΩ. These parameters are used for all the designed experiments.

Since the discharge current has significant effect on the plasma dynamic, electrodynamic, thermodynamic and radiation processes in the plasma focus devices [46], the current wave form and its derivative are used to validate the model as compared with published experimental results [45].

Figure 2 shows the calculated (SPF) and measured total discharge currents (Exp), and Figure 3 shows the corresponding current derivatives for a DT mixture. The used mass fraction f_m is 0.11, the current fraction f_c is 0.68. The current fraction f_c is calculated with the help of the published calculation method [47] as 0.66 and adjusted to 0.68 for better match between experimentally measured discharge current and the calculated discharge current for model validation as follows:

$$I_{peak} = \frac{2\pi C_0 V_0}{\tau}, \quad (34)$$

$$f_c = \frac{I_{exp}}{I_{peak}}, \quad (35)$$

where I_{peak} and I_{exp} are the theoretical and experimental peak discharge current, and τ is the discharge time period [47].

The theoretical calculations have good agreement with the experimental results for both the discharge currents

Fig. 3. Current derivatives corresponding to the discharge currents in Figure 2 for DT mixture.

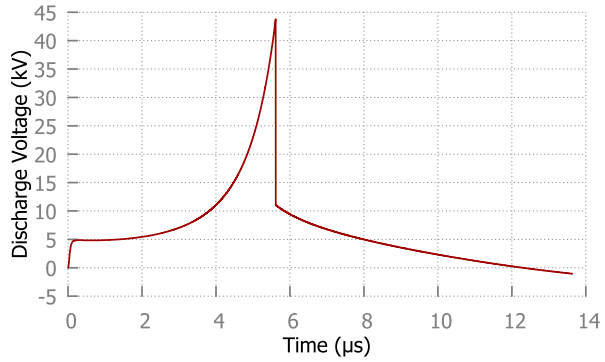

Fig. 4. Discharge voltage for DT mixture.

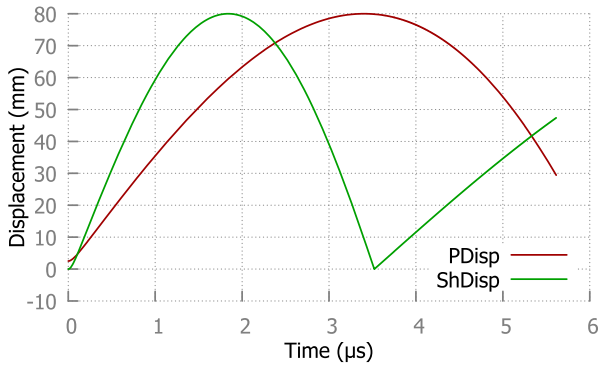

Fig. 5. Plasma and shock front displacements for DT mixture.

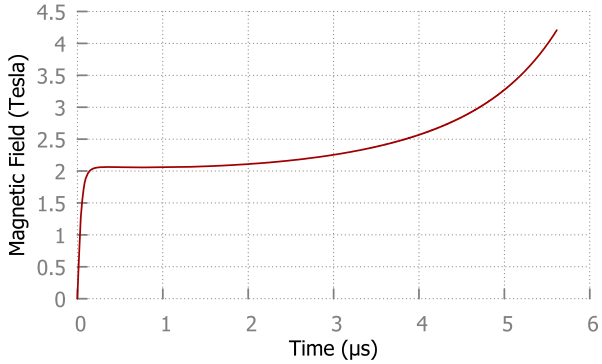

Fig. 6. Magnetic field for DT mixture.

and the current derivatives. The smaller sharp value in the model prediction of the current derivative is mainly due to the use of constant f_m and f_c in the model for all the phases, while it could be variable in the experiment for each small time interval. Another possible reason may be attributed to gas breakdown before the CS starts moving, which has considerable effect on the discharge current. The current sheet motion in the experiment starts after the gas breakdown, while this time delay in the current sheet motion in the model is not taken into account, which results in a slight difference between the model and the experimental results [25].

3.2 Plasma parameters for DT mixture

Figure 4 shows the discharge voltage of the SPF. The sharper the voltage spike, the deeper the discharge current dip, the better the focus in the plasma focus devices [48,49]. Therefore, the sharp voltage spike at 5.6 μs with the maximum discharge voltage of 43.7 kV in Figure 4 and the discharge current dip of 910 kA from the maximum discharge current of 1446 kA in Figure 2 are indications for a good focus in the SPF.

Figure 5 shows the displacement of the plasma (the CS) and the shock front from the axis. Since the geometry is spherical, both the CS and shock front displacements are increasing from the first antipodal point until the equator point of the spherical shape. While the shock front reaches the maximum displacement at 1.84 μs, it takes 3.4 μs for the CS. Slug thickness also increases due to higher speed of the shock front. Since the distance from the axis are decreasing from the equator point to the other antipodal point and both the CS and shock front moves along the axis, the displacements start decreasing with increasing slug thickness. The shock front moves with higher speed and it reaches the axis at 3.5 μs then reflects back towards the CS by decreasing the slug thickness while the CS still moves towards the axis with decreasing displacement. The CS and reflected shock meets at 41.7 mm away from the axis at 5.3 μs.

Figure 6 shows the induced magnetic field due to the flowing current, as previously expressed by the set of equations, in which the magnetic field depends on the current and the distance of the CS from the axis. It roughly depends on the ratio of $\frac{I}{r}$ where r is the distance from the axis for the CS, and I is the discharge current. Since both the discharge current and the distance from the axis are increasing, and the ratio stays almost the same, the magnetic field does not change much from beginning to 3.5 μs of the motion which is the time when the shock front hits the axis and reflects back towards the CS. It also corresponds to both the close-to-maximum discharge current and the time when the CS just passed the equator point of the sphere which is the end of the rundown phase I. After rundown phase I, the magnetic field starts increasing until the point where the CS and the reflected shock front meets.

Figure 7 shows the velocity of the CS, and Figure 8 shows the velocity of the shock front and the reflected

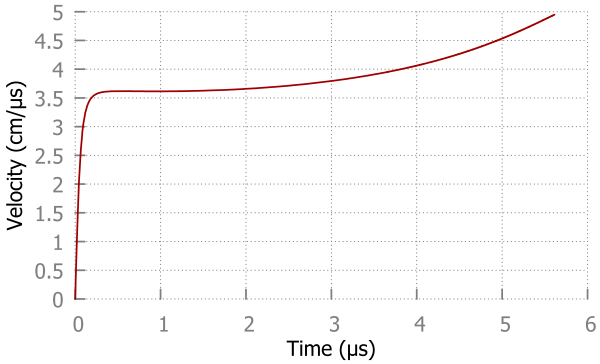

Fig. 7. Plasma velocity for DT mixture.

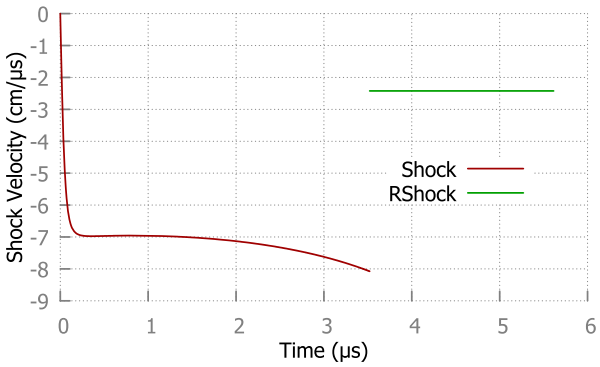

Fig. 8. Shock front velocities for DT mixture.

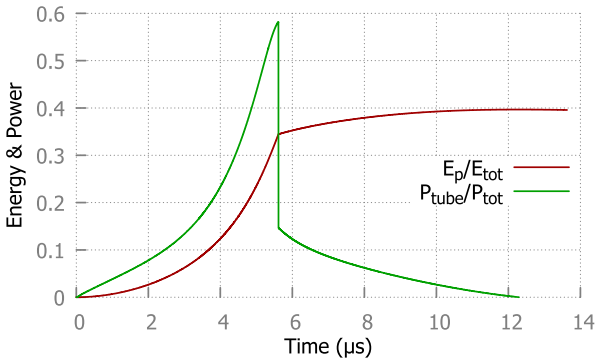

Fig. 9. Tube power and plasma sheath energy.

shock front (RShock). The shock velocity starts increasing as shown in Figure 8 in the beginning of the motion. Therefore, temperature starts increasing until the shock front hits the axis. After this point, there is a plateau in the temperature which is due to the assumed constant reflected shock front velocity as seen in the Figure 8.

The CS velocity is increasing until the CS hits the reflected shock front, and a constant reflected shock front velocity is assumed after the shock front hits the axis. While plasma velocity follows the same trajectory as magnetic field because magnetic field drives the plasma slug, the shock velocity follows the same trajectory as the temperature because shock velocity increases the temperature by ionizing the gases in front of the plasma slug.

Figure 9 shows the energy deposited into the plasma sheath normalized to total energy ($E_p/E_{\rm tot}$) and the power deposited into the tube normalized to total power ($P_{\rm tube}/P_{\rm tot}$). The total energy $E_{\rm tot}$ from equation (24) and the total power $P_{\rm tot}$ from equation (25) are calculated as 135 kJ and 68.46 GW. While the maximum deposited energy into the plasma sheath at the end of the motion is about 54 kJ which is equal to approximately 40% of the total energy, the maximum deposited power into the tube at 5.6 μs is 39.84 GW which is 58% of the total power as in Figure 9. Since 39.84 GW is 58% of the total power deposited into tube, multiplying 0.58 by f_c factor of 0.68 results in 39.44% which is approximately the same as the deposited energy into plasma. Therefore, it can be deduced that 39.44% of the total power, which is 27 GW, can be deposited into the plasma. The point where E_p starts saturating and $P_{\rm tube}$ reach the maximum value occur at 5.6 μs.

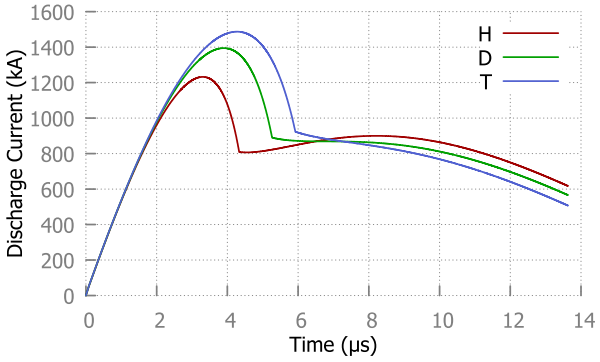

Fig. 10. Discharge currents for H, D and T.

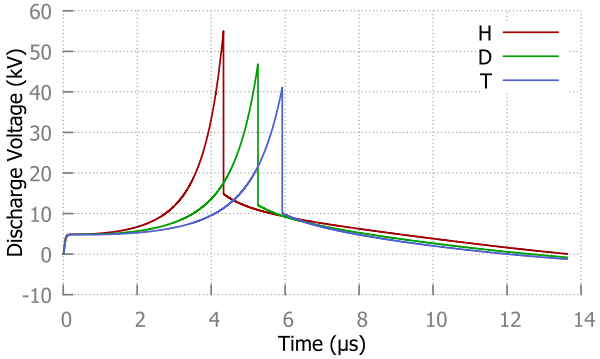

Fig. 11. Discharge voltages for H, D and T.

3.3 Plasma parameters for hydrogen, deuterium and tritium SPF

The variations of the discharge current and discharge voltage with respect to time for hydrogen, deuterium and tritium are shown in Figures 10 and 11, respectively for charging voltage of 25 kV.

As can be seen from Figure 10 the peak discharge currents are 1.232 MA at 3.304 μs for hydrogen, 1.394 MA at 3.897 μs for deuterium and 1.487 MA at 4.271 μs for tritium. Dip discharge currents are 809 kA at 4.333 μs for hydrogen, 890 kA at 5.264 μs for deuterium and 923 kA at 5.922 μs for tritium. Dip discharge currents occur at the

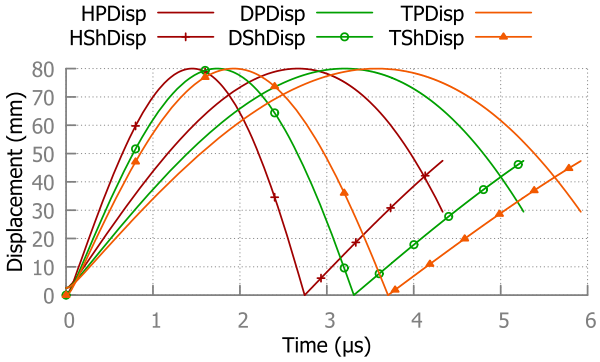

Fig. 12. Plasma and shock front displacements for H, D and T.

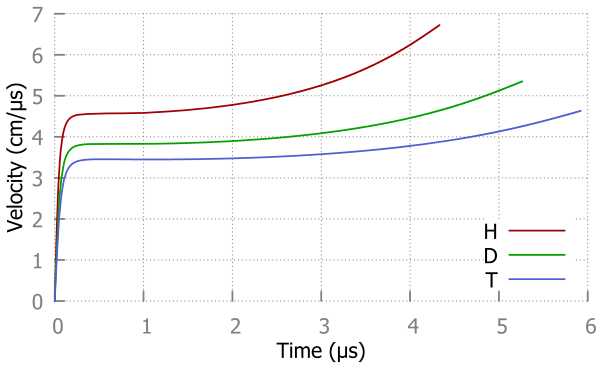

Fig. 13. Plasma velocities for H, D and T.

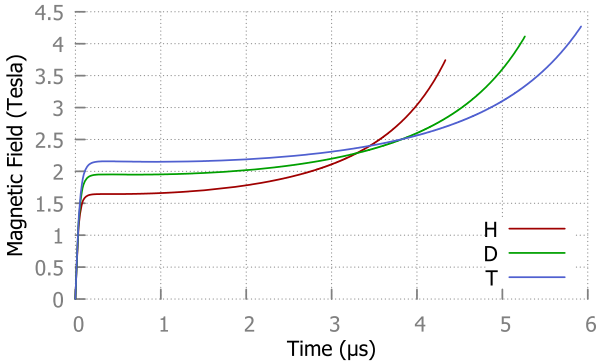

Fig. 14. Magnetic fields for H, D and T.

same time with the peak discharge voltage (Fig. 11).The peak discharge voltages are 55 kV at 4.333 μs for hydrogen, 46.85 kV at 5.264 μs for deuterium and 41 kV at 5.922 μs for tritium. As the molecular weight of the gas increases the peak discharge current also increases, but peak discharge voltage decreases. Since deeper discharge current and sharper discharge voltage result in better focus in the dense plasma focus devices [48,49], then a better focus can be achieved by using hydrogen which is the lightest gas as compared to deuterium and tritium for the same conditions in the sense that hydrogen has the deepest discharge current dip and the highest discharge voltage spike.

The displacement of the CS and shock front are shown in Figure 12 for hydrogen, deuterium and tritium. HPDisp, DPDisp and TPDisp represent plasma displacement(or the CS displacement), for hydrogen, deuterium and tritium, respectively. HShDisp, DShDisp and TShDisp represent the shock front displacement for the corresponding gases.

In case of hydrogen, while shock front reaches the equator point at 1.45 μs, it takes 2.67 μs for the CS. For deuterium, the time to reach the equator point is 1.73 μs for the shock front and 3.2 μs for the CS. For tritium, it takes 1.93 μs for the shock front to move from the beginning to the end of the half sphere as the CS reaches this point at 3.57 μs. As the molecular weight of the gas is increased, the time from beginning to the point where the CS and shock front meets is also increased as well as the time to reach the equator point for the CS and shock front, and the time to hit the axis for the shock front. The effect of the molecular weight of the gas on the plasma velocity can be seen in Figure 13 as well. Interesting point about the CS and shock front displacement is the time it takes to reach both equator point for the CS and shock front, and axis for the shock front when molecular weight is increased. The CS and shock front hit each other approximately at the same distance from the axis for hydrogen, deuterium and tritium as well as for DT mixture. The distances from the axis are 41.7 mm for hydrogen, deuterium, tritium and DT mixture.

Figure 14 shows the magnetic field due to the current flow. Since magnetic field follows the plasma velocity, and the rate of change in the plasma velocity is increasing after the CS finishes the rundown phase I, the magnetic fields for each gases also increases after this point where the CS reaches the equator point of the spherical plasma focus.

4 Conclusions

The snow plow model, shock wave equations and equivalent circuit model for dense plasma focus were used in this study to develop a simulation regime of a spherical plasma focus (SPF) device with two concentric spheres. The model provides results including plasma parameters for hydrogen, deuterium and tritium comparable to experimental published data. The simulation determined the effect of the variation of the gas pressure, discharge voltage and the gas molecular weight on plasma temperature and pinch start time as well as the effect of the gas molecular weight on the plasma parameters.

The SPF model results showed good agreement with the experimental data for the discharge current and its derivative, with good accuracy, which are the main indicators to show how well the plasma focus model compares well to the experiment.

In order to obtain plasma and shock wave parameters with respect to molecular mass of the gas, discharge voltage and gas pressure, several computational runs were completed for hydrogen, deuterium, tritium and DT mixture by varying the filling gas type, filling gas pressure and discharge voltage.

While the maximum discharge current achieved is 1.487 MA with tritium, the maximum voltage peak and the deepest discharge current dip are 55 kV and 809 kA respectively with hydrogen which makes hydrogen a better candidate, compared to deuterium and tritium, to have a good focus in dense plasma focus devices. An interesting finding is the point where the CS and reflected shock front meets as displacement in that the CS and reflected shock front meets at approximately the same distance from the axis for all the cases.

The obtained temperature variation in terms of the gas pressure and discharge voltage with different gas types suggests that the maximum plasma temperature can be achieved with a heavier gas by using low filling gas pressure and high discharge voltage. After the reflected shock front hits the CS at the end of the reflected shock phase, the radiative phase starts, which is not yet included in this model, therefore, the effect of the radiation emission is not calculated herein and will be included in future work. The radiation emission can result in energy gain with the joule heating and energy losses with the bremsstrahlung and line radiation, which also affects the temperature. Maximum deposited energy into the plasma sheath E_p and the maximum deposited power into the tube are around 40% of the total energy $E_{\rm tot}$ and 58% of the total power, respectively, without including the effect of the radiation emission.

References

1. N.V. Filippov, T.I. Filippova, V.P. Vinogradov, Nucl. Fusion Suppl. **2**, 577 (1962)
2. J.W. Mather, Phys. Fluids **7**, S28 (1964)
3. J.W. Mather, Phys. Fluids **8**, 366 (1965)
4. M. Zakaullah, G. Murtaza, S. Qamar, I. Ahmad, M. Beg, Phys. Scripta **53**, 360 (1996)
5. M. Zakaullah, I. Ahmad, G. Murtaza, M. Beg, Fusion Eng. Des. **36**, 437 (1997)
6. S. Lee, S.H. Saw, J. Fusion Energ. **27**, 292 (2008)
7. S. Lee, S.H. Saw, Appl. Phys. Lett. **92** (2008)
8. S. Lee, P. Lee, S.H. Saw, R.S. Rawat, Plasma Phys. Contr. F. **50**, 065012 (2008)
9. A. Serban, S. Lee, J. Plasma Phys. **60**, 3 (1998)
10. A. Serban, S. Lee, Fusion Technol. **35**, 54 (1999)
11. J. Koh, R. Rawat, A. Patran, T. Zhang, D. Wong, S. Springham, T. Tan, S. Lee, P. Lee, Plasma Sources Sci. T. **14**, 12 (2005)
12. J. Pouzo, M. Milanese, IEEE Trans. Plasma Sci. **31**, 1237 (2003)
13. A.A. Zaeem, IEEE Trans. Plasma Sci. **38**, 2069 (2010)
14. S. Knecht, R. Thomas, F. Mead, G. Miley, D. Froning, in *AIP Conference Proceedings* (2006), Vol. 813, p. 1232
15. S. Lee, in *Proceedings of College Plasma Phys., Trieste, Italy* (1983), p. 967
16. S. Lee, in *Proceedings of the first Tropical College on Applied Physics: "Laser and Plasma Technology, Kuala Lumpur, Malaysia* (1985), pp. 3–36
17. S. Lee, in *Proceedings of the first Tropical College on Applied Physics: "Laser and Plasma Technology, Kuala Lumpur, Malaysia* (1985), pp. 37–62
18. S. Lee, C.S. Wong, T.Y. Tou, J.B. Ali, A. Chew, in *Proceedings of the first Tropical College on Applied Physics: "Laser and Plasma Technology, Kuala Lumpur, Malaysia* (1985), pp. 63–90
19. S. Lee, in *Proceedings of the first Tropical College on Applied Physics: "Laser and Plasma Technology, Kuala Lumpur, Malaysia* (1985), pp. 379–386
20. M.M. Masoud, H.A. El-Gamal, H.A. El-Tayeb, A.A. Hassouba, M. A. Abd Al-Halim, Plasma Dev. Oper. **15**, 263 (2007)
21. J. Gonzalez, A. Clausse, H. Bruzzone, P. Florido, IEEE Trans. Plasma Sci. **32**, 1383 (2004)
22. J. Gonzalez, M. Barbaglia, F. Casanova, A. Clausse, Braz. J. Phys. **39**, 633 (2009)
23. M. Mathuthu, T. Zengeni, A. Gholap, IEEE Trans. Plasma Sci. **25**, 1382 (1997)
24. T.D. Mahabadi, M.A. Tafreshi, Plasma Phys. Cont. F **49**, 1447 (2007)
25. V. Siahpoush, M. Tafreshi, S. Sobhanian, S. Khorram, Plasma Phys. Contr. F. **47**, 1065 (2005)
26. S. Goudarzi, R. Amrollahi, R.S. Moghaddam, J. Fusion Energ. **27**, 195 (2008)
27. D.E. Potter, Phys. Fluids **14**, 1911 (1971)
28. D. Potter, Nucl. Fusion **18**, 813 (1978)
29. B. Shan, P. Lee, S. Lee, Sing. J. Phys. **16**, 25 (2000)
30. P. Lee, A. Serban, IEEE Trans. Plasma Sci. **24**, 1101 (1996)
31. A. Márquez, J. González, A. Tarifeno-Saldivia, C. Pavez, L. Soto, A. Clausse, Phys. Plasmas **19**, 012703 (2012)
32. F. Casanova, A. Tarifeño-Saldivia, F. Veloso, C. Pavez, A. Clausse, L. Soto, J. Fusion Energy **31**, 279 (2012)
33. F. Casanova, H. Bruzzone, A. Clausse, IEEE Trans. Plasma Sci. **40**, 2312 (2012)
34. F. Casanova, C. Moreno, A. Clausse, Plasma Phys. Control. Fusion **47**, 1239 (2005)
35. C. Moreno, F. Casanova, G. Correa, A. Clausse, Plasma Phys. Control. Fusion **45**, 1989 (2003)
36. M.A. Abd Al-Halim, J. Fusion Energy **29**, 134 (2010)
37. S. Al-Hawat, M. Soukieh, M.A. Kharoub, W. Al-Sadat, Vacuum **84**, 907 (2010)
38. G. Murtaza, S. Hussain, N. Rehman, S. Naseer, M. Shafiq, M. Zakaullah, Surf. Coat. Technol. **205**, 3012 (2011)
39. R. Verma, R. Rawat, P. Lee, M. Krishnan, S.V. Springham, T. Tan, IEEE Trans. Plasma Sci. **38**, 652 (2010)
40. H. Khan, M. Shafiq, S. Hussain, M. Zakaullah, J. Appl. Phys. **107**, 073301 (2010)
41. M. Habibi, R. Amrollahi, G. Etaati, J. Fusion Energy **29**, 49 (2010)
42. R. Niranjan, R. Rout, P. Mishra, R. Srivastava, A. Rawool, T. Kaushik, S.C. Gupta, Rev. Sci. Instrum. **82**, 026104 (2011)
43. M. Krishnan, IEEE Trans. Plasma Sci. **40**, 3189 (2012)
44. S. Lee, J. Fusion Energy **33**, 319 (2014)
45. N.V. Zavyalov, V.V. Maslov, V.G. Rumyantsev, I.Y. Drozdov, D.A. Ershov, D.S. Korkin, D.A. Molodtsev, V.I. Smerdov, A.P. Falin, A.A. Yukhimchuk, Plasma Phys. Rep. **39**, 243 (2013)
46. L. Sing, S. Sor Heoh, Energies **3**, 711 (2010)
47. S. Saw, S. Lee, F. Roy, P. Chong, V. Vengadeswaran, A. Sidik, Y. Leong, A. Singh, Rev. Sci. Instrum. **81**, 053505 (2010)
48. M. Hosseinnejad, Z. Ghorannevis, M. Ghoranneviss, M. Soltanveisi, M. Shirazi, J. Fusion Energy **30**, 516 (2011)
49. N. Fani, H. Savaloni, J. Theor. Appl. Phys. **6**, 1 (2012)